2014-02-03

Disconnected quark loop contributions to nucleon observables in lattice QCD

Abdel-Rehim, A

10.1103/physrevd.89.034501
Physical Review D
American Physical Society (APS)

Disconnected quark loop contributions to nucleon observables in lattice QCD

A. Abdel-Rehim[(a)], C. Alexandrou [(a,b)], M. Constantinou [(b)], V. Drach [(c)], K. Hadjiyiannakou [(b)], K. Jansen [(b,c)], G. Koutsou [(a)], A. Vaquero [(a)]
[(a)] *Computation-based Science and Technology Research Center, Cyprus Institute, 20 Kavafi Street, Nicosia 2121, Cyprus*
[(b)] *Department of Physics, University of Cyprus, P.O. Box 20537, 1678 Nicosia, Cyprus*
[(c)] *NIC, DESY, Platanenallee 6, D-15738 Zeuthen, Germany*
(Dated: January 7, 2014)

We perform a high statistics calculation of disconnected fermion loops on Graphics Processing Units for a range of nucleon matrix elements extracted using lattice QCD. The isoscalar electromagnetic and axial vector form factors, the sigma terms and the momentum fraction and helicity are among the quantities we evaluate. We compare the disconnected contributions to the connected ones and give the physical implications on nucleon observables that probe its structure.

PACS numbers: 11.15.Ha, 12.38.Gc, 12.38.Aw, 12.38.-t, 14.70.Dj

I. INTRODUCTION

Lattice QCD simulations are currently performed near or at the physical value of the light quark mass. This allows a study of hadron structure that can provide valuable information for phenomenology and experiment. However, a number of important observables are computed neglecting disconnected quark loop contributions. The evaluation of disconnected quark loops is therefore of paramount importance if we want to eliminate a systematic error inherent in the determination of hadron matrix elements in lattice QCD. The computation of disconnected quark loops within the lattice QCD formulation requires the calculation of the so-called all-to-all or time-slice-to-all propagators, for which the computational resources required to estimate them with, e.g. stochastic methods, are much larger than those required for the corresponding connected contributions. In addition, they are prone to large gauge noise. It is for these reasons that in most hadron structure studies up to now the disconnected contributions were neglected, introducing an uncontrolled systematic uncertainty [1].

Recent progress in algorithms, however, combined with the increase in computational power, have made such calculations feasible. On the algorithmic side, a number of improvements like the one-end trick [2–4], dilution [5–9], the Truncated Solver Method (TSM) [9–11] and the Hopping Parameter Expansion (HPE) [2, 12] have led to a significant reduction in both stochastic and gauge noise associated with disconnected quark loops. Moreover, using special properties of the twisted mass fermion Lagrangian [13–16] one can further enhance the signal-to-noise ratio by taking the appropriate combination of flavors. On the hardware side, graphics cards (GPGPUs or GPUs) can provide a large speedup in the evaluation of quark propagators and contractions. In particular, for the TSM, which relies on a large number of inversions of the Dirac matrix in single or half precision, GPUs provide an optimal platform.

In this paper, the aim is to use our findings on the performance of recently developed methods [17] to compute to high accuracy the disconnected contributions that enter in the determination of nucleon form factors, sigma terms and first moments of parton distributions. The evaluation will be performed using one ensemble generated with two light degenerate quarks and a strange and charm quark with masses fixed to their physical values ($N_f = 2 + 1 + 1$) using the twisted mass fermion discretization. The lattice size is $32^3 \times 64$, the lattice spacing extracted from the nucleon mass [18] $a = 0.082(1)(4)$ fm and the pion mass about 370 MeV. This ensemble will be hereafter referred to as the B55.32 ensemble. The aim is to compare the disconnected contributions computed using $\mathcal{O}(10^5)$ measurements to the connected ones and assess the importance of the disconnected contributions to nucleon observables computed in lattice QCD for this given ensemble. The paper is organized as follows: in Section II we summarize the algorithms and variance reduction techniques employed, and in Section III we present the main numerical results of this paper, namely the disconnected contributions to nucleon generalized form factors. In Section IV we compare the disconnected contributions with the corresponding connected ones. In Section V we give our conclusions and outlook.

II. METHODS FOR DISCONNECTED CALCULATIONS

A. Truncated Solver Method

The exact computation of all-to-all (or time-slice-to-all) propagators on a lattice volume of physical interest is outside our current computer power, since this would require volume (or spatial volume) times inversions of the Dirac matrix, whose size ranges from $\sim 10^7$ for a $24^3 \times 48$ lattice to $\sim 10^9$ for the largest volumes of $96^3 \times 192$ considered nowadays. We will use the Truncated Solver Method (TSM) combined with the one-end trick to evaluate the disconnected contributions. This method was shown to be optimal for most observables involved in nucleon structure computations [17]. For completeness

we summarize here the methods and refer the reader to Ref. [17] for a more detailed description and the comparison against other methods.

The usual approach to evaluate disconnected contributions is to compute an unbiased stochastic estimate of the all-to-all propagator [19] by generating a set of N_r sources $|\eta_r\rangle$ randomly drawn from e.g. $\mathbb{Z}_2 \otimes i\mathbb{Z}_2$. Solving for $|s_r\rangle$ in

$$M\,|s_r\rangle = |\eta_r\rangle \tag{1}$$

and calculating

$$M_E^{-1} := \frac{1}{N_r}\sum_{r=1}^{N_r} |s_r\rangle\,\langle\eta_r| \approx M^{-1} \tag{2}$$

provides an unbiased estimate of the all-to-all propagator as $N_r \to \infty$. Since, in general, the number of noise vectors N_r required is much smaller than the lattice volume V, the computation becomes feasible. How large N_r should be depends on the observable.

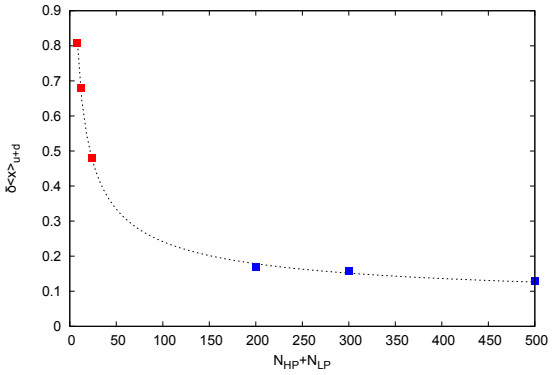

FIG. 1: The error on the isoscalar momentum fraction $\delta\langle x\rangle_{u+d}$ as a function of $N_{\rm HP} + N_{\rm LP}$ for 68000 measurements. The three leftmost points (red squares) correspond to $N_{\rm LP} = 0$ and the three rightmost to $N_{\rm HP} = 24$. The dotted line is the result of fitting to the Ansatz $1/\sqrt{a + \frac{b}{N_{\rm HP}+N_{\rm LP}}}$.

The TSM is a way to increase N_r at a reduced computational cost. The idea behind the method is the following: instead of inverting to high precision the stochastic sources in Eq. (1), we can aim at a low precision (LP) estimate

$$|s_r\rangle_{LP} = \left(M^{-1}\right)_{LP} |\eta_r\rangle\,, \tag{3}$$

where the number of inversions of the Conjugate Gradient (CG) used is truncated. The criterion for the low precision inversions can be selected by specifying a relaxed stopping condition in the CG e.g. by allowing a relatively large value of the residual, which in turn determines the number of iterations required to invert a source to low precision. Following Refs. [9, 17], we choose a stopping condition at fixed value of the residual $|\hat{r}|_{\rm LP} \sim 10^{-2}$. $N_{\rm HP}$ is then selected by requiring that the bias introduced when using $N_{\rm LP}$ low precision vectors is corrected. We estimate the correction C_E to the bias stochastically by inverting a number of sources to high and low precision, and calculating the difference,

$$C_E := \frac{1}{N_{\rm HP}}\sum_{r=1}^{N_{\rm HP}} \left[|s_r\rangle_{\rm HP} - |s_r\rangle_{\rm LP}\right]\langle\eta_r|\,, \tag{4}$$

where the $|s_r\rangle_{\rm HP}$ are calculated by solving Eq. (1) up to high precision, so our final estimate becomes

$$\begin{aligned} M^{-1}_{E_{TSM}} := & \frac{1}{N_{\rm HP}}\sum_{r=1}^{N_{\rm HP}} \left[|s_r\rangle_{\rm HP} - |s_r\rangle_{\rm LP}\right]\langle\eta_r| \\ & + \frac{1}{N_{\rm LP}}\sum_{j=N_{\rm HP}}^{N_{\rm HP}+N_{\rm LP}} |s_r\rangle_{\rm LP}\,\langle\eta_r|\,, \end{aligned} \tag{5}$$

which requires $N_{\rm HP}$ high precision (HP) inversions and $N_{\rm HP} + N_{\rm LP}$ low precision inversions. The ratio of the number of HP inversions to the LP ones is determined with the criterion of choosing as large a ratio as possible while still ensuring that the final result is unbiased. In this work, we will compute fermion loops with the complete set of Γ-matrices up to one-derivative operators. The tuning is, thus, performed using an operator that requires a large number of stochastic noise vectors, such as the nucleon isoscalar momentum fraction $\langle x\rangle_{u+d}$ and we optimize $N_{\rm HP}$ and $N_{\rm LP}$ so as to get the smallest error at the lowest computational cost. In Fig. 1 we show the error on $\langle x\rangle_{u+d}$ as one varies $N_{\rm HP}$ and $N_{\rm LP}$. As can be seen, the error decreases like $1/\sqrt{a + \frac{b}{N_{\rm HP}+N_{\rm LP}}}$ with a and b positive parameters. Fixing $N_{\rm HP} = 24$ and increasing $N_{\rm LP}$ reduces the error rapidly until $N_{\rm LP}$ reaches about $N_{\rm LP} \sim 300$. In Ref. [17] we showed that a ratio of $N_{\rm LP}$ to $N_{\rm HP}$ of about 20 can be considered sufficient to produce an unbiased estimate for the class of observables considered here. Therefore, in this work we take $N_{\rm HP} = 24$ and choose $N_{\rm LP} = 500$ for the light quark sector. For the strange and charm quarks we take $N_{\rm LP} = 300$. These values were shown to also be optimal for the isoscalar axial charge [17].

B. The one-end trick

The twisted mass fermion (TMF) formulation allows the use of a very powerful method to reduce the variance of the stochastic estimate of the disconnected diagrams. From the discussion given in section II A, the standard way to proceed with the computation of disconnected diagrams would be to generate N_r stochastic sources η_r, invert them as indicated in Eq. (1), and compute the disconnected diagram corresponding to an operator X as

$$\frac{1}{N_r}\sum_{r=1}^{N_r}\left\langle \eta_r^\dagger X s_r\right\rangle \;=\; \mathrm{Tr}\left(M^{-1}X\right) \;+\; O\left(\frac{1}{\sqrt{N_r}}\right), \tag{6}$$

where the operator X is expressed in the twisted basis. However, if the operator X involves a τ_3 acting in flavor space, one can utilize the following identity of the twisted mass Dirac operator with $+\mu$ denoted by M_u and $-\mu$ denoted by M_d:

$$M_u - M_d = 2i\mu a\gamma_5. \tag{7}$$

Inverting this equation we obtain

$$M_u^{-1} - M_d^{-1} = -2i\mu a M_d^{-1}\gamma_5 M_u^{-1}. \tag{8}$$

Therefore, instead of using Eq. (6) for the operator $X\tau_3$, we can alternatively write

$$\begin{aligned}&\frac{2i\mu a}{N_r}\sum_{r=1}^{N_r}\left\langle s_r^\dagger\gamma_5 X s_r\right\rangle = \\ &\mathrm{Tr}\left(M_u^{-1}X\right) - \mathrm{Tr}\left(M_d^{-1}X\right) + O\left(\frac{1}{\sqrt{N_r}}\right) = \\ &-2i\mu a\mathrm{Tr}\left(M_d^{-1}\gamma_5 M_u^{-1}X\right) + O\left(\frac{1}{\sqrt{N_r}}\right).\end{aligned} \tag{9}$$

Two main advantages result due to this substitution: i) the fluctuations are effectively reduced by the μ factor, which is small in current simulations, and ii) an implicit sum of V terms appears in the right hand side (rhs) of Eq. (8). The trace of the left hand side (lhs) of the same equation develops a signal-to-noise ratio of $1/\sqrt{V}$, but thanks to this implicit sum, the signal-to-noise ratio of the rhs becomes $V/\sqrt{V^2}$. In fact, using the one-end trick yields for the same operator a large reduction in the errors for the same computational cost as compared to not using it [2–4]. A similar approach proved to be very successful in the determination of the η' mass [20–22]. The identity given in Eq. (8) can only be applied when a τ_3 flavor matrix appears in the operator expressed in the twisted basis. For other operators one can use the identity

$$M_u + M_d = 2D_W, \tag{10}$$

where D_W is the Dirac-Wilson operator without a twisted mass term. After some algebra, one finds

$$\frac{2}{N_r}\sum_{r=1}^{N_r}\left\langle s_r^\dagger\gamma_5 X\gamma_5 D_W s_r\right\rangle \;=\; \mathrm{Tr}\left(M_u^{-1}X\right) + \mathrm{Tr}\left(M_d^{-1}X\right) \;+\; O\left(\frac{1}{\sqrt{N_r}}\right). \tag{11}$$

This lacks the μ-suppression factor, which, as we will see in the following sections and as discussed in more detail in Ref. [17], introduces a considerable penalty in the signal-to-noise ratio.

Because of the volume sum that appears in Eq. (8) and Eq. (11), the sources must have entries on all sites, which in turn means that we can compute the fermion loop at all time slices where the operator is inserted in a single inversion. This allows us to evaluate the three-point function for all combinations of source-sink time separation and insertion time slices, which will prove essential in identifying the contribution of excited state effects for the different operators.

III. RESULTS

In this section we present results from a high statistics evaluation of all the disconnected contributions involved in the evaluation of nucleon form factors and first moments of generalized parton distributions as well as sigma terms. As already mentioned, the analysis is performed using an ensemble of $N_f = 2+1+1$ twisted mass configurations simulated with pion mass of $am_\pi = 0.15518(21)(33)$ and strange and charm quark masses fixed to approximately their physical values (B55.32 ensemble) [23]. The lattice size is $32^3\times 64$ giving $m_\pi L \sim 5$. We use the one-end trick method combined with the TSM with $N_{\rm HP} = 24$ and $N_{\rm LP} = 500$ noise vectors for the light quark loops. For the strange and charm quark sector we use $N_{\rm HP} = 24$ and $N_{\rm LP} = 300$. Using 2,300 gauge-field configurations, with 16 source positions for the two-point function and by averaging results for the proton/neutron and forward/backward propagating nucleons we effectively have $\sim 150,000$ measurements.

An advantage of the one-end trick is that, having the loop at all time slices, we can combine with two-point functions produced at any source time slice. Furthermore, since the noise sources are defined on all sites, we obtain the fermion loops at all insertion time slices. We can thus compute all possible combinations of source-sink time separations and insertion times in the three-point function. This feature enables us to use the summation method, in addition to the plateau method, with no extra computational effort.

The summation method has been known for a long time [24, 25] and has been revisited in the study of g_A [26]. In both the plateau and summation approaches, one constructs ratios of three- to two-point functions in order to cancel unknown overlaps and exponentials in the leading contribution such that the matrix element of the ground state is isolated. For general momentum transfer we consider the ratio

$$R(t_{\rm ins},t_s)=\frac{G^{3pt}(\Gamma^\nu,\vec{p},\vec{q},t_{\rm ins},t_s)}{G^{2pt}(\vec{p}',t_s)}\sqrt{\frac{G^{2pt}(\vec{p},t_s-t_{\rm ins})G^{2pt}(\vec{p}',t_{\rm ins})G^{2pt}(\vec{p}',t_s)}{G^{2pt}(\vec{p}',t_s-t_{\rm ins})G^{2pt}(\vec{p},t_{\rm ins})G^{2pt}(\vec{p},t_s)}} \tag{12}$$

where the two- and three-point functions are given respectively by

$$G^{2pt}(\vec{q},t_s) = \sum_{\vec{x}_s} e^{-ix_s\cdot\vec{q}}\,\Gamma^0_{\beta\alpha}\,\langle J_\alpha(t_s,\vec{x}_s)\overline{J}_\beta(0,\vec{0})\rangle \tag{13}$$

$$G^{3pt}(\Gamma^\nu,\vec{p},\vec{q},t_{\rm ins},t_s) = \sum_{\vec{x}_{\rm ins},\vec{x}_s} e^{i\vec{x}_{\rm ins}\cdot\vec{q}}\,e^{-i\vec{x}_s\cdot\vec{p}}\,\Gamma^\nu_{\beta\alpha}\,\langle J_\alpha(t_s,\vec{x}_s)\mathcal{O}^{\mu_1\cdots\mu_n}(t_{\rm ins},\vec{x}_{\rm ins})\overline{J}_\beta(0,\vec{0})\rangle\,. \tag{14}$$

$q = p' - p$ is the momentum transfer, t_s is the time separation between the sink and the source with the source taken at zero, and $t_{\rm ins}$ the time separation between the current insertion and the source. We consider the complete set of operators $\mathcal{O}^{\mu_1,\cdots,\mu_n}$ up to one derivative, namely the scalar $\bar\psi\,\psi$, vector $\bar\psi\,\gamma^\mu\psi$, axial-vector $\bar\psi\,\gamma^5\,\gamma^\mu\psi$ and the tensor $\bar\psi\sigma^{\mu\nu}\psi$ currents, and the one-derivative vector $\bar\psi\,\gamma^{\{\mu_1}D^{\mu_2\}}\psi$ and axial-vector $\bar\psi\,\gamma_5\,\gamma^{\{\mu_1}D^{\mu_2\}}\psi$ operators. We consider kinematics for which the final momentum $\vec{p}' = 0$ when we consider the connected contributions. For the evaluation of disconnected contributions we use kinematics where $\vec{p} = \vec{p}' \neq 0$ as well as $\vec{p}' = 0$. The projection matrices Γ^0 and Γ^k are given by:

$$\Gamma^0 = \frac{1}{4}(\mathbb{1}+\gamma_0)\,,\quad \Gamma^k = \Gamma^0 i\gamma_5\sum_{k=1}^{3}\gamma_k\,. \tag{15}$$

For zero momentum transfer the ratio simplifies to

$$R(t_{ins},t_s) = \frac{G^{3pt}(\Gamma^\nu,\vec{p},t_{ins},t_s)}{G^{2pt}(t,\vec{p})} \tag{16}$$

The leading time dependence of the ratio $R(t_{\rm ins},t_s)$ is given by

$$R(t_{ins},t_s) = R_{GS} + O(e^{-\Delta E_K t_{ins}}) + O(e^{-\Delta E_K(t_s-t_{ins})}), \tag{17}$$

where R_{GS} is the matrix element of interest, and the other contributions come from the undesired excited states of energy difference ΔE_K. In the plateau method, one plots $R(t_{ins},t_s)$ as a function of $t_{\rm ins}$. For large time separations $t_{\rm ins}$ and $t_s - t_{\rm ins}$ when excited state effects are negligible this ratio becomes a constant (plateau region) and therefore fitting it to a constant yields R_{GS}. In the alternative summation method, one performs a sum over $t_{\rm ins}$ to obtain:

$$R_{\rm sum}(t_s) = \sum_{t_{\rm ins}=0}^{t_{\rm ins}=t_s} R(t_{\rm ins},t_s) = t_s R_{GS} + a + O(e^{-\Delta E_K t_s}) \tag{18}$$

where a is a constant and the exponential contributions coming from the excited states decay as $e^{-\Delta E_K t_s}$ as opposed to the plateau method where excited states are suppressed like $e^{-\Delta E_K(t_s-t_{ins})}$, with $0 \le t_{\rm ins} \le t_s$. Therefore, we expect a better suppression of the excited states for the same t_s. Note that one can exclude from the summation the initial and final time slices t_s and 0 without affecting the dependence on t_s in Eq. (18). The results given in this work are obtained excluding these contact terms from the summation. The drawback of the summation method is that one requires knowledge of the three point function for all insertion times and multiple sink times and one needs to fit to a straight line with two fitting parameters instead of one.

Z_A	Z_T	Z_P	$Z_{DV}^{\mu\mu}$	$Z_{DV}^{\mu\neq\nu}$	$Z_{DA}^{\mu\mu}$	$Z_{DA}^{\mu\neq\nu}$
0.757(3)	0.769(1)	0.506(4)	1.019(4)	1.053(11)	1.086(3)	1.105(2)

TABLE I: Renormalization constants in the chiral limit at $\beta = 1.95$ in the $\overline{\rm MS}$-scheme at $\mu = 2$ GeV. Z_A, Z_T and Z_P are the renormalization constants for the axial-vector, tensor and scalar currents, and Z_{DV} and Z_{DA} for the one-derivative vector and axial-vector operators $\mathcal{O}^{\mu\nu}$. The errors given are statistical.

Before comparing the lattice matrix elements $R_{\rm GS}$ with experiment we need to renormalize them. We denote the renormalized ratio by $\tilde{R}(t_{\rm ins},t_s)$. Regarding the renormalization of the sigma terms, the twisted mass formulation has the additional advantage of avoiding any mixing, even though we are using Wilson-type fermions [4]. For the case of the axial charge, renormalization involves mixing from the three quark sectors. For the tree-level Symanzik improved gauge action this mixing was shown to be a small effect of a few percent [27]. We expect this to hold also for the Iwasaki action used in this work and for the other isoscalar quantities. In this work, we neglect the small difference in the renormalization constant between connected and disconnected contributions and we use the same renormalization constants as for the connected piece. They are given in Table I. The value of Z_P needs a pole subtraction and is taken from Ref. [28, 29], while all the others have been calculated using the approach given in Refs. [30, 31]. All the renormalization constants, except Z_A which is scheme and scale independent, are converted from RI-MOM to $\overline{\rm MS}$ at a scale

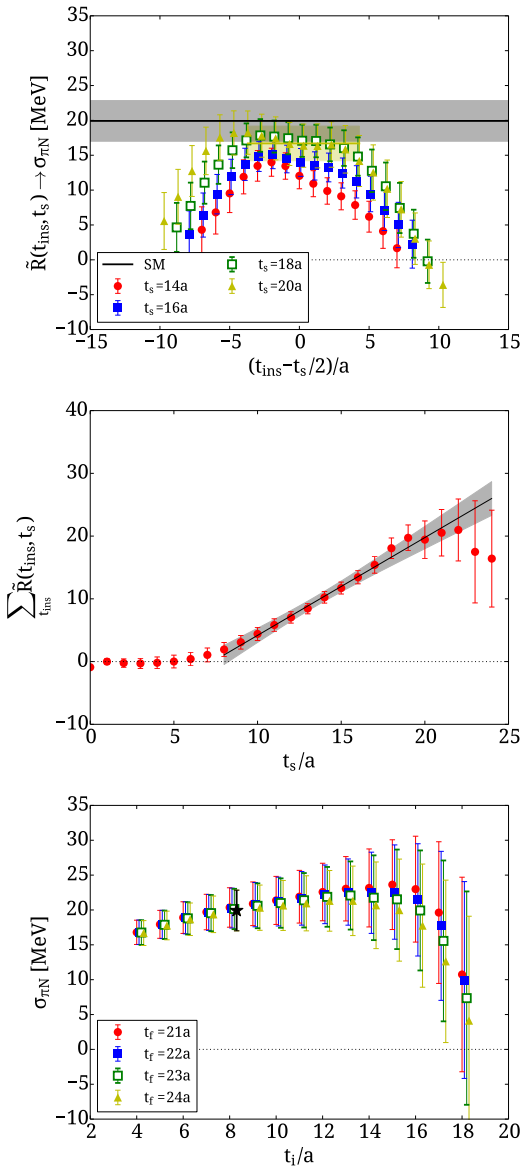

FIG. 2: The disconnected contribution to the ratio from which $\sigma_{\pi N}$ is extracted. On the upper panel we show the ratio as a function of the insertion time slice with respect to the mid-time separation $(t_{\rm ins} - t_s/2)$ for source-sink time separations, $t_{\rm s}$ =14a (red filled circles), $t_{\rm s} = 16a$ (blue filled squares), $t_{\rm s} = 18a$ (green open squares) and $t_{\rm s} = 20a$ (yellow filled triangles). In the central panel we show the summed ratio, for which the fitted slope yields the desired matrix element. On the lower panel we show the results obtained for the fitted slope of the summation method for various choices of the initial and final fit time slices. The star shows the choice for which the gray bands are plotted in the upper and central panels.

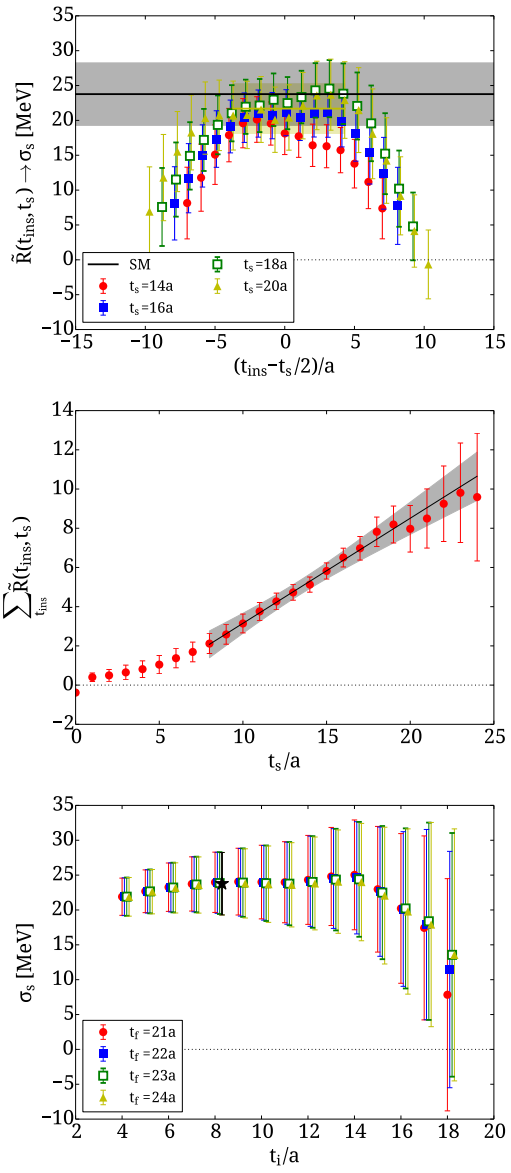

FIG. 3: The ratio from which the strange quark content of the nucleon, σ_s, is extracted. The notation is the same as that of Fig. 2.

of $\mu = 2$ GeV. The conversion factors for Z_T are taken from Ref. [32], and for the one-derivative operators from Ref. [30], computed to three-loops. We remark that in the twisted basis the scalar charge is renormalized with Z_P.

In Fig. 2 we show the results for the disconnected contribution to the ratio from which the $\sigma_{\pi N}$-term is extracted. The ratio is plotted versus the time separation of the current insertion $t_{\rm ins}$ from the source, shifted by $t_s/2$. When this ratio becomes time independent (plateau region) fitting to a constant yields $\sigma_{\pi N}$. As can be seen, however, increasing the source-sink time separation increases the value extracted from fitting to the plateau (plateau value). We observe that one requires a source-sink time separation of at least 18 to 20 time slices in order for the plateau value to stabilize. This is a distance of $\gtrsim 1.5$ fm, which is significantly larger than the nominal source-sink separation of 1.0 fm-1.2 fm typically used in nucleon matrix element calculations. In the cen-

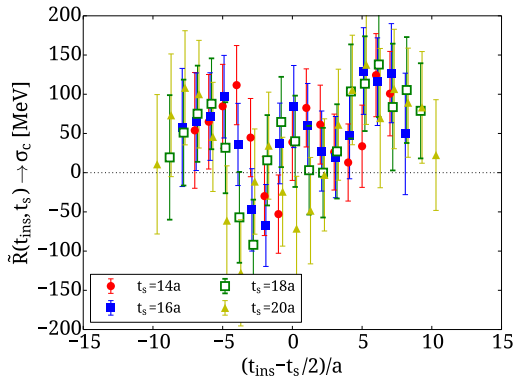

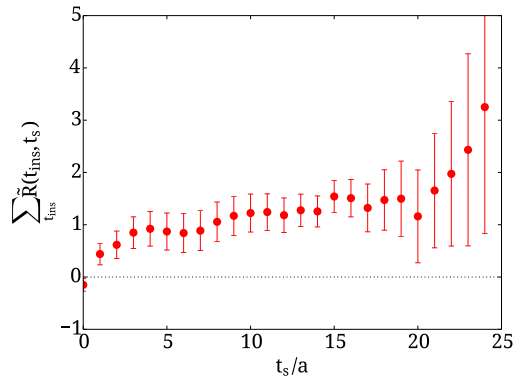

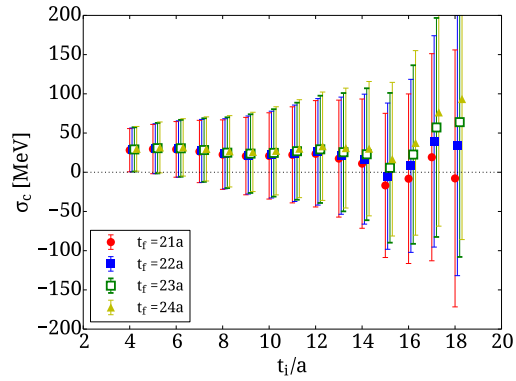

FIG. 4: The ratio from which the charm quark content of the nucleon, σ_c, is extracted. The notation is the same as that of Fig. 2.

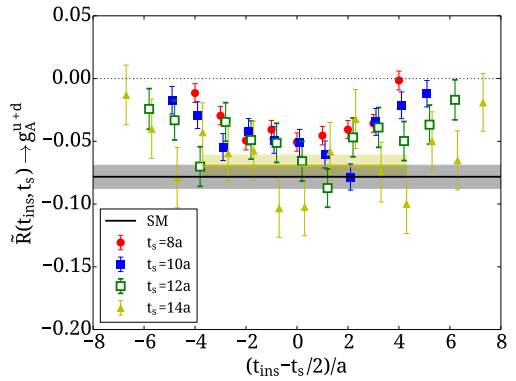

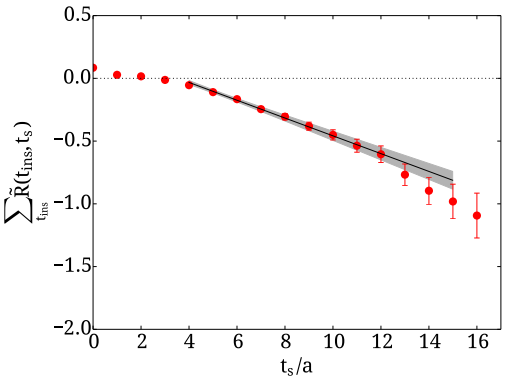

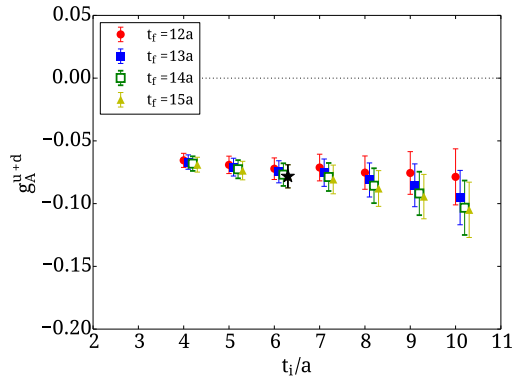

FIG. 5: The disconnected contribution to the renormalized ratio which yields the isoscalar axial charge of the nucleon, g_A^{u+d}. The upper panel shows the ratio as a function of the insertion time slice with respect to the mid-time separation $(t_{\rm ins} - t_s/2)$ for source-sink separations $t_{\rm s} = 8a$ (red filled circles), $t_{\rm s} = 10a$ (blue filled squares), $t_{\rm s} = 12a$ (green open squares) and $t_{\rm s} = 14a$ (yellow filled triangles). The central panel shows the summed ratio and the lower panel the results obtained for the fitted slope of the summation method for various choices of the initial and final fit time slices as explained in the text. The star shows the choice of t_i, which yields the gray bands shown in the upper and central plots.

tral panel we show the ratio summed over the insertion time slice as given in Eq. (18) referred to as summation method (SM) as a function of the source-sink time separation time. As explained earlier, by fitting the ratio to a straight line one obtains the desired matrix element as the slope. This is done for several choices of the initial and final fit time slices (t_i and t_f respectively) with the results displayed in the lower panel of the figure. As one increases the initial fit time slice the excited state contributions are expected to become smaller and thus the fitted value stabilizes. Note, however, that the slope changes and one needs to vary the fit range until the slope converges. Therefore, if one has only a small number of source-sink time separations one may miss the variation of the slope. As in the case of the plateau method where we take the smallest t_s for which excited states are sufficiently suppressed, it is desirable to take the smallest t_i for which the excited states no longer contribute significantly, since the error to signal ratio increases with

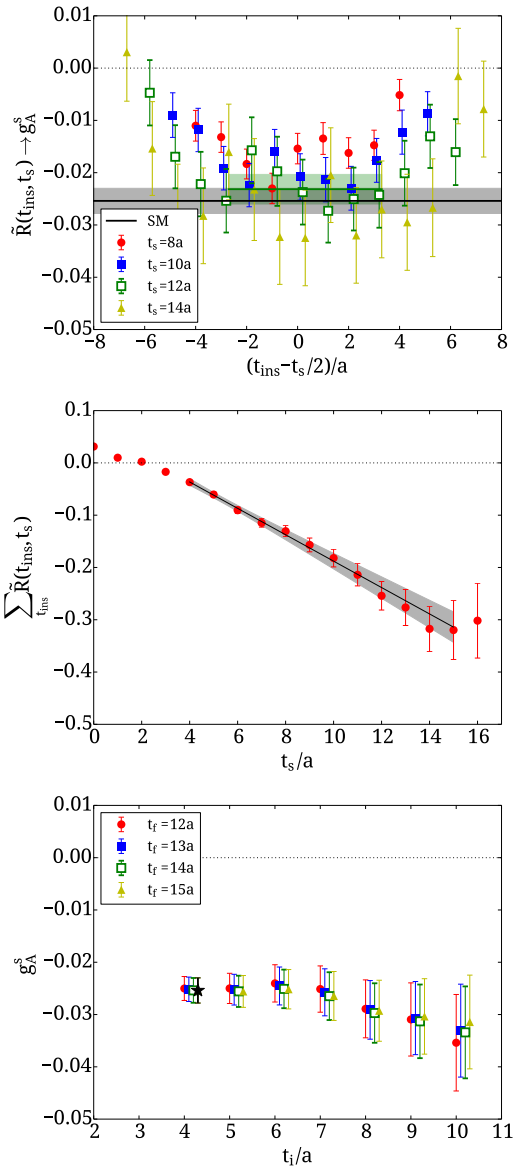

FIG. 6: The strange-quark contribution to the renormalized ratio yielding the nucleon axial charge g_A^s. The notation is the same as that of Fig. 5.

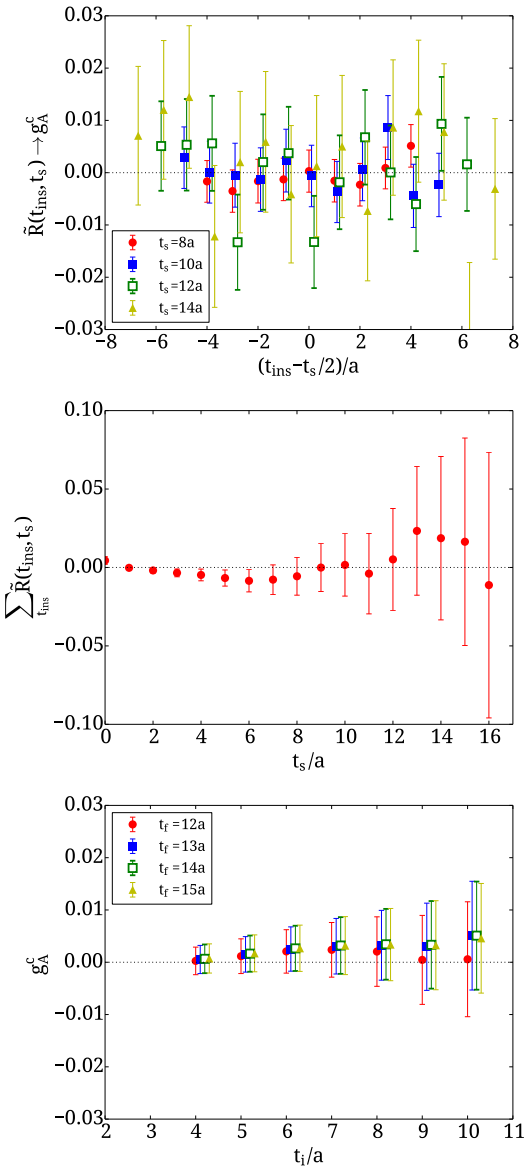

FIG. 7: The charm-quark contribution to the renormalized ratio yielding the nucleon axial charge g_A^c. The notation is the same as that of Fig. 5.

t_i. Taking the value of the slope to be the one given by the star yields the value of $\sigma_{\pi N}$ shown by the gray band in the upper panel of the figure. As can be seen, the resulting value is in agreement with the (colored) band obtained from the plateau method for $t_s/a = 20$.

A similar analysis is undertaken for the strange- and charm-quark sigma terms, shown in Figs. 3 and 4 respectively. For σ_s, similar remarks can be made as in the case of $\sigma_{\pi N}$, most notably concerning the large source-sink separation required for the plateau method to converge. As expected, the results between the summation and the plateau method are consistent also in this case, when excited states are suppressed. Non-zero results for σ_s were also obtained in Ref. [33] using optimal noise sources and low-mode substitution techniques. For the case of the charm content, our results are consistent with zero both when using the plateau method as well as when using the summation method allowing us only to obtain an upper bound to its value. In Ref. [33] a non-zero result was obtained as one approaches the chiral limit. Since our aim in this work is to compute quark loops using high statistics for one ensemble we will address the quark mass dependence in a follow-up work.

Similar analyses are carried out for the disconnected contributions entering the ratios determining the nucleon axial charge. For observables like g_A where one does not have the τ^3 flavor combination in the twisted basis it is advantageous to use the discrete symmetries of the

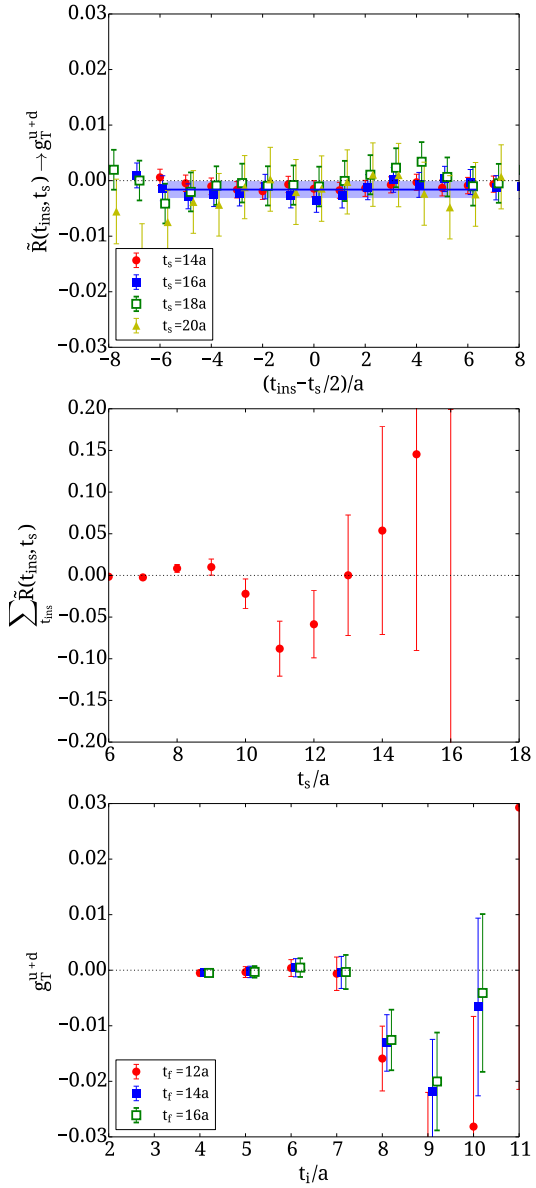

FIG. 8: The disconnected contribution to the renormalized ratio yielding the nucleon isoscalar tensor charge g_T^{u+d}. The notation is the same as that of Fig. 2.

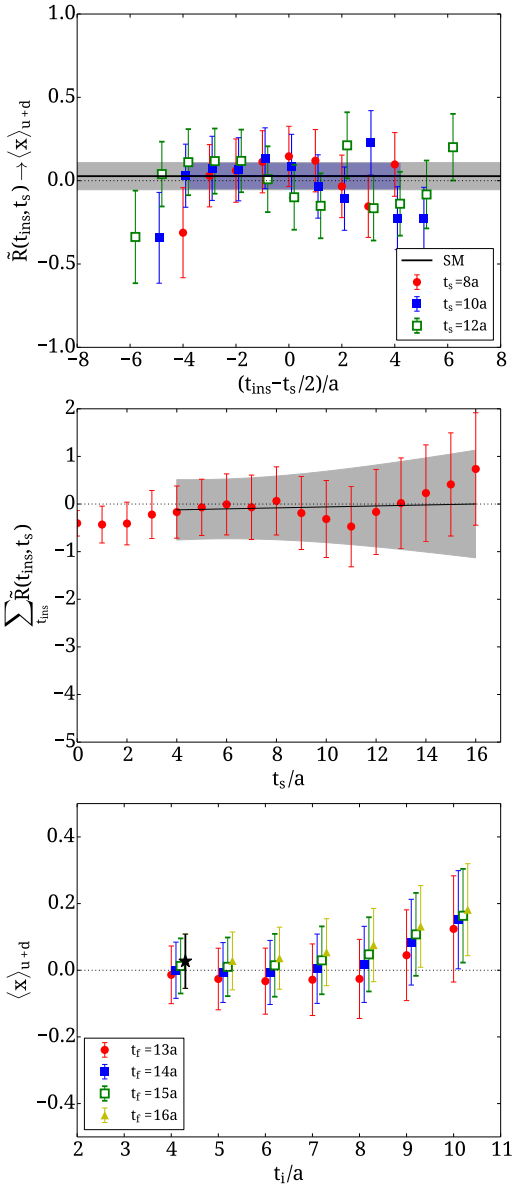

FIG. 9: The disconnected contribution to the renormalized ratio yielding the nucleon isoscalar momentum fraction $\langle x \rangle_{u+d}$. The notation is the same as that of Fig. 5.

twisted mass formulation [15, 16], namely parity combined with isospin flip $u \leftrightarrow d$, γ_5-isospin hermiticity, and charge-γ_5-isospin hermiticity, in order to reduce gauge noise. Considering the properties of the quark loops and of the nucleon two-point functions that enter in the computation of the disconnected three-point function under these symmetries one can derive appropriate products taking their real or imaginary parts thus suppressing gauge noise. This was shown to be advantageous in the calculation of the first moments of the unpolarized momentum distribution in Ref. [34]. These symmetries are used for the results shown from now on. In Figs. 5, 6 and 7 we show, respectively, results for the ratio from which the nucleon matrix elements of the axial-vector current yielding the isoscalar g_A,the strange g_A^s and the charm g_A^c are extracted. We first note that for the case of g_A^{u+d} we observe less contamination from excited states than in the case of the sigma terms. This is evident from the smaller source-sink time separations required in order for the plateau or summation method to converge. Furthermore, we clearly observe a non-zero value for the case of the disconnected contributions to the isoscalar g_A as well as for g_A^s. For g_A^c our results are consistent with zero and we can only give an upper bound to its value. The nucleon tensor charge g_T^{u+d} is also computed and the ratio from which is extracted is shown in Fig 8. We observe a very small value for the disconnected contribution, with an error of about 90%. For the summation method the

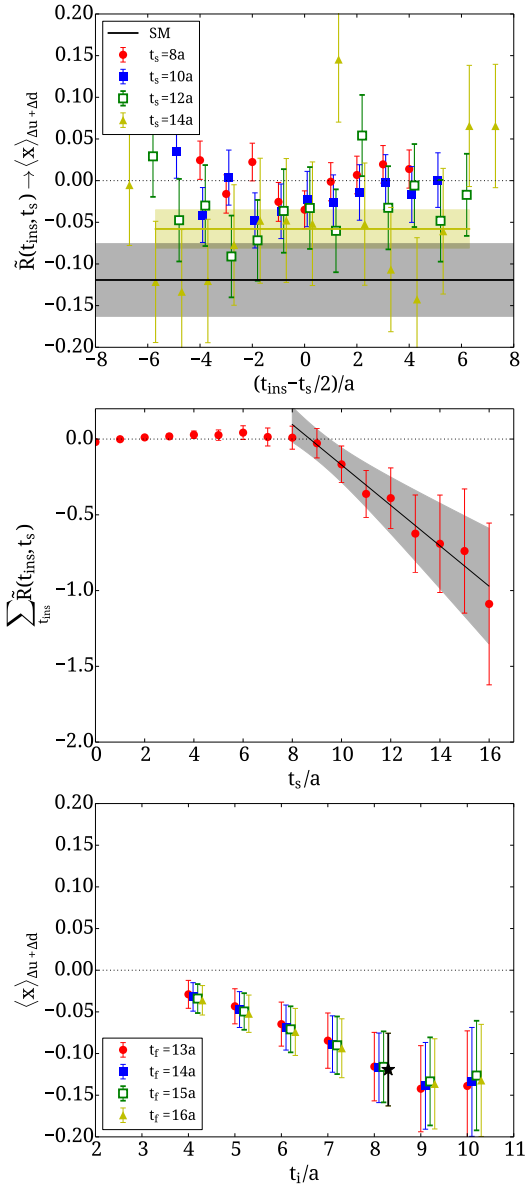

FIG. 10: The disconnected contribution to the renormalized ratio yielding nucleon isoscalar helicity moment $\langle x \rangle_{\Delta u+\Delta d}$. The notation is the same as that of Fig. 5.

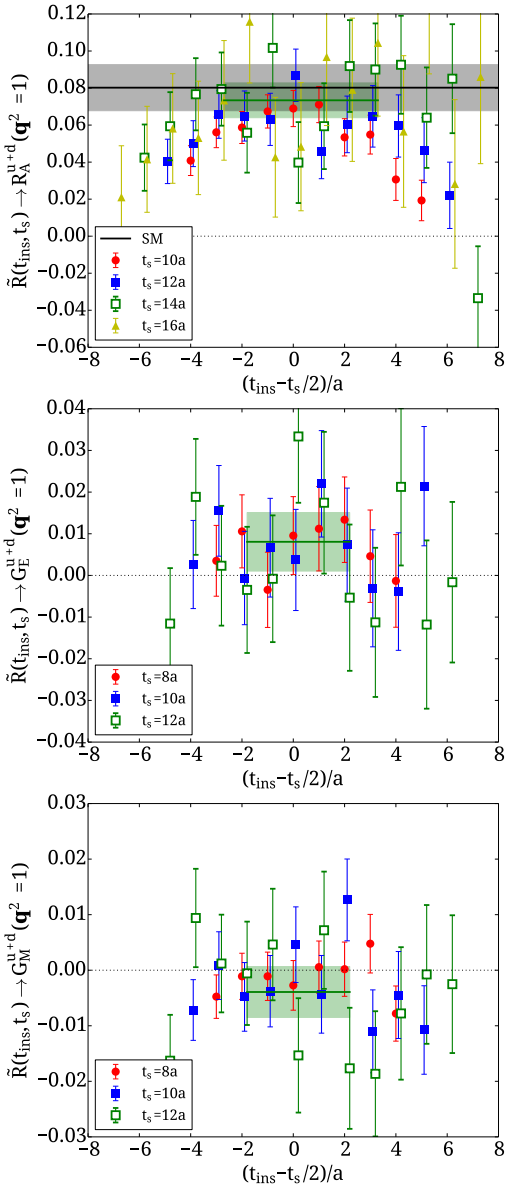

FIG. 11: Disconnected contributions to the renormalized ratio yielding the isoscalar axial-vector and pseudo-scalar form-factors G_A and G_p (upper), the electric form-factor G_E (center) and the magnetic form-factor G_M (lower) at the lowest non-zero momentum transfer allowed for this lattice size.

statistical uncertainty does not allow a meaningful fit.

The nucleon matrix elements involving derivative operators probe moments of parton distributions, which are extracted from deep inelastic scattering measurements. In this work we compute the disconnected contributions to the isoscalar nucleon momentum fraction $\langle x \rangle_{u+d}$, which involves the vector derivative operator and the isoscalar nucleon polarized moment $\langle x \rangle_{\Delta u+\Delta d}$ involving the axial-vector derivative operator. We apply the symmetries of the twisted mass action discussed above as well as consider a moving frame and thus have the nucleon carrying non-zero equal initial and final momentum for three-point functions with zero momentum transfer. We find that, when the nucleon carries the lowest momentum allowed for this lattice, the statistical error is reduced. The disconnected contributions to the ratios, from which the matrix elements of the vector and axial-vector derivative operators, are extracted are shown in Figs. 9 and 10 respectively. For $\langle x \rangle_{u+d}$ we find a value consistent with zero both with the plateau and summation method. Having one unit of momentum improves the signal enabling us to deduce an upper bound on the value of this matrix element. For $\langle x \rangle_{\Delta u+\Delta d}$ the statistical errors remain large but nevertheless we obtain a non-zero value. Considering a moving nucleon leads in this particular case to a substantial reduction in the error. We note

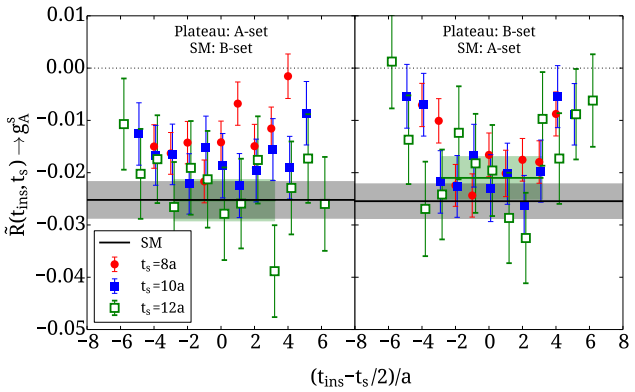

FIG. 12: The renormalized ratio which yields the strange-quark contribution to the axial charge of the nucleon, g_A^s. In the left panel, the plateau method is used on the first half of the ensemble (A-set), while the summation method is used on the second half of the ensemble (B-set). In the right panel, he plateau method is used on the A-set, while the summation method is used on the B-set.

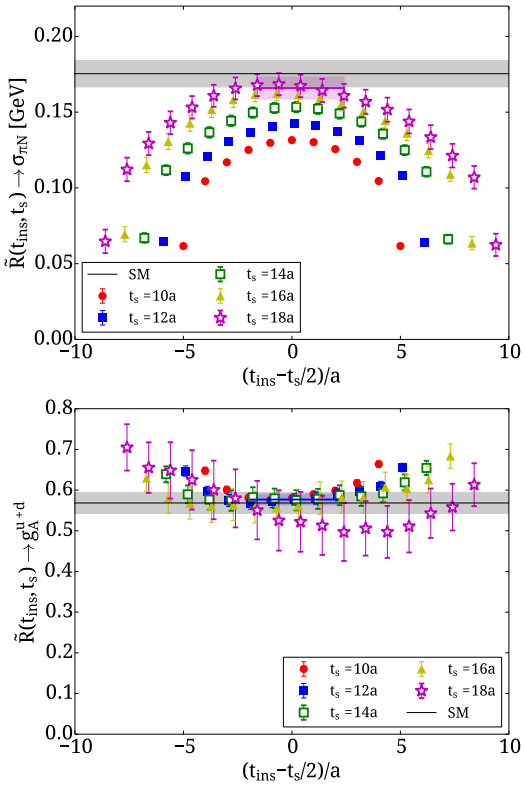

FIG. 13: Connected contributions to the ratio yielding $\sigma_{\pi N}$ (upper) and nucleon isoscalar axial charge (lower), for various source-sink time separations are shown. Results obtained from a fit to a constant to the ratio (colored band) and from a linear fit to the summed ratio (gray band) are also displayed.

.

that increasing the sink-source time separation is crucial in order for this observable to develop a non-zero result. This is clearly seen in the slope which becomes non-zero for $t_s/a > 8$. Since a large t_s also leads to larger errors it is no surprise that such a large number of statistics is needed to obtain a meaningful signal. This may also indicate that even larger number of statistics are needed to stabilize further the signal.

Apart from matrix elements for zero momentum transfer presented so far, disconnected contributions arise in the isoscalar electromagnetic and axial form factors at finite momentum. Computationally, these are straightforward to extract, since one takes the Fourier transform of the insertion coordinate of the loop to obtain the matrix element at all momenta. The finite momentum matrix elements, however, are expected to be nosier than the zero-momentum ones, since the energy factors appearing in the exponents of the signal are larger. The disconnected contributions to the axial form-factors, electric form-factor and magnetic form-factor are shown in Fig. 11 for a single unit of momentum transfer. Due to the structure of the matrix elements and the way these are computed on the lattice, for the case of the axial form factors G_A and G_p, the plot shows the ratio of a linear combination from which these form factors are extracted after the plateau fit. G_E and G_M, on the other hand, can be extracted from different ratios allowing us to plot them separately. We note that we perform a similar analysis for these quantities as for the zero-momentum case where both plateau and summation methods are investigated for the optimal fit ranges. For the axial form-factors we obtain a clearly non-zero value. For the electromagnetic case, the disconnected contributions for both the isoscalar electric and magnetic form factors are statistically consistent with zero.

Finally we comment on the issue of correlations. The summation and plateau methods for various quantities are compared using the same set of gauge configurations and found to be consistent. Since these results can be correlated, the difference between the results of the two methods maybe underestimated. Thus, it is worthwhile to investigate the two methods using different sets of configurations. To perform this check we split our ensemble into two equal sets, which we will refer to as A-set and B-set, and redo our analysis on these two sets separately. We show the result for the case of the strange-quark contribution to the axial charge in Fig. 12. As can seen, the values computed in each set both using the plateau and summation methods are in agreement. Furthermore, the plateau computed using the A-set is consistent with the summation method computed using the B-set and vice versa. This agreement indicates that the consistency between the results extracted using the summation and plateau methods on the full ensemble is not due to possible correlations.

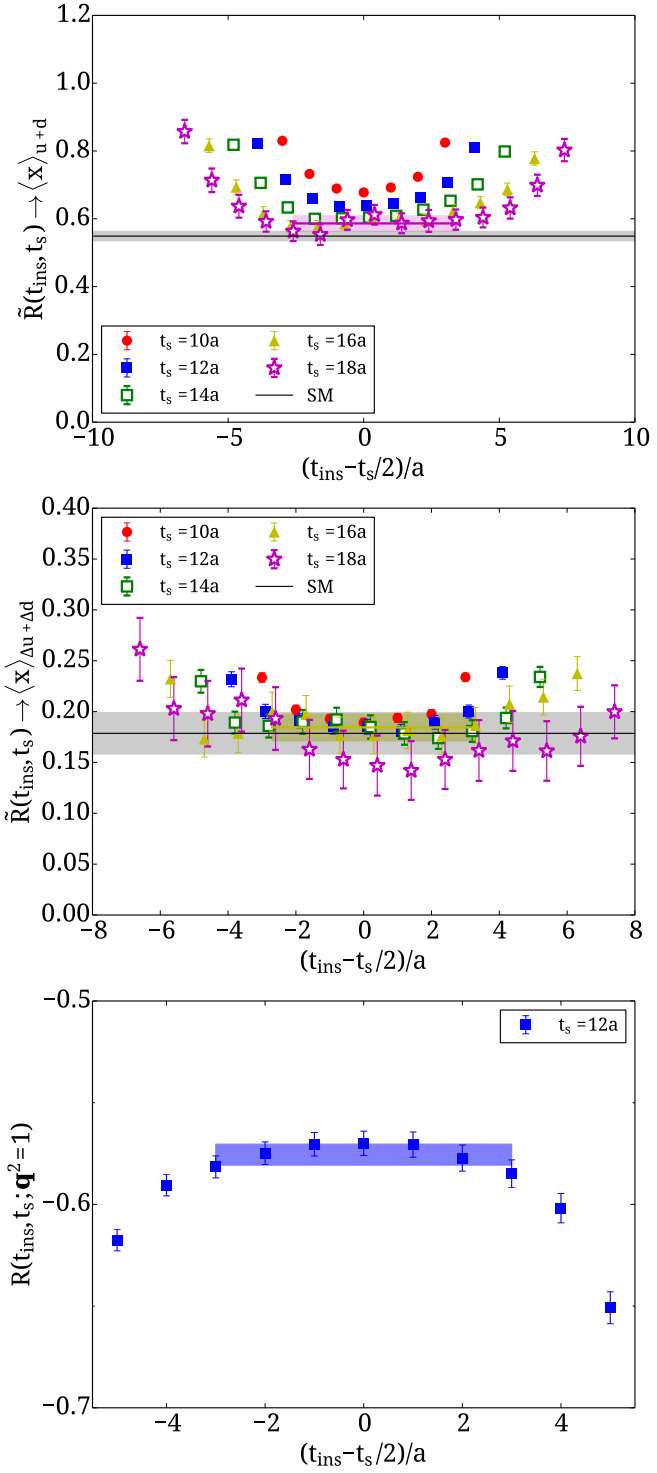

FIG. 14: Connected contributions to the renormalized ratio yielding the isoscalar nucleon momentum fraction (upper), the isoscalar nucleon helicity moment (center) and the axial and pseudo-scalar form factors $G_A(Q^2)$ and $G_p(Q^2)$ at a single unit of momentum (lower) are shown. For the momentum fraction and helicity, we show the results obtained from a fit to a constant to the renormalized ratio (colored band) and from a linear fit to the summed renormalized ratio (gray band).

.

IV. COMPARISON WITH CONNECTED CONTRIBUTION

The main motivation for calculating disconnected fermion loops is to eliminate the systematic uncertainty, which arises when these are omitted from calculations of hadronic matrix elements. For instance, the nucleon axial charge is typically computed in the isovector combination, where the fermion loops of the up- and down-quarks cancel. However, if one is interested in the intrinsic spin fraction carried by the individual quarks, one needs, in addition to the isovector, the isoscalar combination, which involves disconnected diagrams. Typically, in lattice QCD calculations up to now, the disconnected contributions have been omitted. It is, therefore, important to identify how large the contributions of disconnected diagrams are, in order to bound the systematic error introduced when these are neglected.

Observable	connected	disconnected	total
Results at zero momentum transfer ($Q^2 = 0$)			
$\sigma_{\pi N}$ [MeV]	164.6(7.2)	16.6(2.4)	181.3(7.6)
σ_s [MeV]		21.7(3.6)	21.7(3.6)
σ_c [MeV]		16(30)	16(30)
g_S^{u+d}	6.30(27)	0.639(95)	6.94(29)
g_S^s		0.246(41)	0.246(41)
g_A^{u+d}	0.576(13)	-0.0699(89)	0.506(15)
g_A^s		-0.0227(34)	-0.0227(34)
g_T^{u+d}	0.673(13)	-0.0016(14)	0.671(13)
$\langle x \rangle_{u+d}$	0.586(22)	0.027(76)	0.614(80)
$\langle x \rangle_{\Delta u+\Delta d}$	0.1948(51)	-0.058(22)	0.136(23)
J^u	0.2781(94)	-0.076(77)	0.202(78)
J^d	-0.0029(94)	-0.076(77)	-0.078(78)
$\Delta\Sigma^u/2$	0.4273(50)	-0.0174(75)	0.4098(55)
$\Delta\Sigma^d/2$	-0.1389(50)	-0.0174(75)	-0.1564(55)
Results for $\vec{q}^2 = (2\pi/L)^2$ or $Q^2 \simeq 0.19$ GeV^2			
G_E^{u+d}	2.2698(78)	0.024(21)	2.293(22)
G_M^{u+d}	2.088(49)	-0.066(75)	2.022(89)
G_A^{u+d}	0.5155(94)	-0.0564(72)	0.459(11)
G_p^{u+d}	9.81(65)	-1.90(35)	7.90(74)
B_{20}^{u+d}	-0.035(16)	-0.33(29)	-0.36(29)
G_E^p	0.7453(32)	0.0040(58)	0.7493(47)
G_E^n	0.0113(32)	0.0040(58)	0.0153(47)
G_M^p	1.847(28)	-0.011(42)	1.836(31)
G_M^n	-1.151(28)	-0.011(42)	-1.162(31)

TABLE II: The connected and disconnected contributions to the various nucleon observables for the B55.32 ensemble are given in column two and three, whereas column four has the total contribution. The form factors G_E, G_M, G_A and G_p, and generalized form factor B_{20} are given for $\vec{q} = 2\pi/L$. The disconnected contributions were obtained using about 150,000 measurements.

In order to assess the importance of disconnected contributions, we evaluate the connected contributions to the isoscalar matrix elements of the operators discussed in the previous section. In Figs. 13 and 14 we show the renormalized ratios from which the connected part of the isoscalar matrix elements are extracted. These results are obtained using 1200 gauge field configurations and inverted for multiple source-sink time separations to allow applying the summation method. We stress that, for the evaluation of the connected contributions unlike the case of the disconnected, to obtain multiple source-sink time separations one needs to do a new set of inversions for each sink-source time separation.

The multiple source-sink time separations are computed more efficiently by using the EigCG [35, 36] method to deflate the lowest eigenvalues with every new right-hand-side. For the connected contributions shown here, we compute the sequential propagators for eight source-sink time separations, namely from $t_s = 4a$ to $t_s = 18a$ for every even time separation. In addition, the sequential propagators are computed for both unpolarized and polarized nucleon sinks, meaning in total 16 sequential propagators per configuration, or 16×12=192 right-hand-sides are needed, one for each color-spin component. Our EigCG is set up such that ten eigenvalues per right-hand-side are deflated, stopping after a total of 24 right-hand-sides, after which the deflated space is kept constant at 240 eigenvalues for the remaining 168 right-hand-sides. With this setup, and at this pion mass, we observe a speedup of more than 3 times, i.e. the 192 right-hand-sides are computed for the same computational cost needed to compute 64 right-hand-sides when not using EigCG.

The ratios yielding the connected contribution to $\sigma_{\pi N}$, and the isoscalar g_A are shown in Fig. 13. These can be compared with the corresponding ratios yielding the disconnected contributions to $\sigma_{\pi N}$ and isoscalar g_A shown in Figs. 2 and 5, respectively. As can be seen, the behavior of the connected contributions is similar to the disconnected ones, namely the sigma term shows large excited state contamination requiring large sink-source separations whereas in the case of g_A^{u+d} the excited states are negligible even for $t_s/a = 10$. For a better comparison between connected and disconnected contributions we collect the results extracted from the plateau method for all nucleon observables in Table II. The disconnected contribution to the $\sigma_{\pi N}$ and isoscalar g_A are found to be larger than 10% of the connected contribution at this quark mass. Clearly for both $\sigma_{\pi N}$ and g_A^{u+d} these are sizable effects and have to be taken into account. The scalar charge derives from the same matrix element as the sigma term and therefore it also requires inclusion of disconnected contributions. For the case of the momentum fraction, the disconnected contribution is found to be consistent with zero as can be seen in Fig. 9, and therefore we can only give an upper bound to its size to be included in the systematic error of $\langle x \rangle_{u+d}$. For the polarized moment $\langle x \rangle_{\Delta u+\Delta d}$, on the other hand, one obtains a sizable non-zero result. Note that the disconnected contribution is negative decreasing the value of $\langle x \rangle_{\Delta u+\Delta d}$ quite substantially. The disconnected contribution to the tensor charge is essentially zero not affecting its total value.

A comment can also be made for the case of the disconnected contributions to the nucleon form factors computed at non-zero momentum shown in Fig. 11 at a single unit of momentum transfer squared. For the electromagnetic form-factors G_E and G_M, we find that the disconnected contributions are consistent with zero and with magnitude less than 1%. With the connected contributions at this momentum transfer being of $O(1)$, this means that the disconnected contributions will, at most, be at the 1% level. For the case of the axial form factor G_A^{u+d}, the disconnected contribution is about 10% that of the connected and thus, it must be included. In the case of the pseudo-scalar form factor G_p, we find that the disconnected contribution is of similar magnitude as the connected one and thus it is crucial in order to get reliable results for this observable to include the disconnected part.

Having the complete set of isoscalar matrix elements with both connected and disconnected contributions, one can combine with the corresponding isovector matrix elements, which do not depend on disconnected contributions, to obtain the separate quark contributions to nucleon matrix elements. This is done in Table II for all the various quantities considered in this work. Namely, the up- and down-quark contributions to the nucleon spin $\Delta\Sigma^u/2$ and $\Delta\Sigma^d/2$ are obtained by combining the isovector and isoscalar axial charges. Including the disconnected contributions affects the values of the intrinsic spin in particular in the case of the d-quark. In contrast, the values of the nucleon total spin J^u and J^d, obtained by combining the isoscalar and isovector vector generalized form-factors A_{20} and B_{20}, are not affected and the disconnected contributions only contribute an upper bound to the error. Finally, the proton/neutron electric and magnetic form factors $G_E^{p/n}$ and $G_M^{p/n}$ at a single unit of momentum transfer squared, which for this lattice size and quark mass corresponds to $Q^2 \simeq 0.19$ GeV^2, are obtained from the isovector and isoscalar proton electric and proton magnetic form-factors assuming flavor-SU(2) isospin symmetry between up- and down-quarks. Only the value of G_E^n is affected although, within error bars, it is still consistent with the connected value.

V. CONCLUSIONS

The computation of disconnected contributions for flavor singlet quantities has become feasible, due to the development of new techniques to reduce the gauge and stochastic noise, and due to the increase in computational resources. In this work, we use the truncated solver method and the one-end trick on GPUs for the determination of disconnected contributions to the nucleon matrix elements. The usage of GPUs is particularly im-

portant, due to its efficiency in the evaluation of disconnected diagrams using the TSM, since GPUs can yield a large speedup when employing single- and half-precision for the computation of the LP inversions and contractions. The calculation is performed for one ensemble of $N_f = 2 + 1 + 1$ twisted mass fermions using very high statistics. This is necessary in order to reduce the gauge noise and obtain statistically significant results.

The results for all observables are analyzed using both the plateau and the summation methods. A careful analysis of excited states is performed and we find that the methods yield results that are compatible, as expected when excited states contributions are negligible and identification of the fitting ranges in both methods are well selected. Therefore, agreement of the values extracted with the plateau and summation methods provides a good consistency check. Since the one-end trick provides results for all sink-source separations at no additional computational cost, such a check can be always carried out.

Comparison of the connected to the disconnected contributions reveals clearly that the latter are important for a number of observables related to nucleon structure. For the sigma terms and scalar charge the disconnected contributions amount to 10% the total value and thus they must be taken into account. Similarly for the isoscalar axial charge we find more than 10% contributions that must be taken into account in the discussion of the spin carried by quarks in the proton. The disconnected contribution reduces the value of Σ^d by more than 10%, an effect that is important if we aim at a few % accuracy. On the other hand, we find that the disconnected contributions to the electromagnetic form factors at low q^2-values are less than 1% at this pion mass. For the axial form factor G_A the disconnected contributions are sizable and persist at the level of 10% of the value of the connected contribution even at non-zero momentum-transfer. For G_p the disconnected contribution is even larger reaching 20%.

In the future we plan to compute the disconnected contributions to these quantities using simulations at physical pion mass. Such a computation will require very large computational resources in order to obtain results with meaningful statistical errors.

Acknowledgments

A. V. and M. C. are supported by funding received from the Cyprus Research Promotion Foundation under contracts EPYAN/0506/08 and and TECHNOLOGY/ΘΕΠΙΣ/0311(BE)/16 respectively. K. J. is partly supported by RPF under contract ΠΡΟΣΕΛΚΥΣΗ/ΕΜΠΕΙΡΟΣ/0311/16. This research was in part supported by the Research Executive Agency of the European Union under Grant Agreement number PITN-GA-2009-238353 (ITN STRONGnet) and the infrastructure project INFRA-2011-1.1.20 number 283286 (HadronPhysics3), and the Cyprus Research Promotion Foundation under contracts ΚΥ-ΓΑ/0310/02 and NEA ΥΠΟΔΟΜΗ/ΣΤΡΑΤΗ/0308/31 (infrastructure project Cy-Tera, co-funded by the European Regional Development Fund and the Republic of Cyprus through the Research Promotion Foundation). Computational resources were provided by the Cy-Tera machine and Prometheus (partly funded by the EU FP7 project PRACE-2IP under grant agreement number: RI-283493) of CaSToRC, Forge at NCSA Illinois (USA), Minotauro at BSC (Spain), and by the Jugene Blue Gene/P machine of the Jülich Supercomputing Center awarded under PRACE.

[1] C. Alexandrou, Prog.Part.Nucl.Phys. **67**, 101 (2012), 1111.5960.
[2] P. Boucaud et al. (ETM), Comput. Phys. Commun. **179**, 695 (2008), 0803.0224.
[3] C. Michael and C. Urbach (ETM Collaboration), PoS **LAT2007**, 122 (2007), 0709.4564.
[4] S. Dinter et al. (ETM Collaboration), JHEP **1208**, 037 (2012), 1202.1480.
[5] S. Bernardson, P. McCarty, and C. Thron, Comput.Phys.Commun. **78**, 256 (1994).
[6] J. Viehoff et al. (TXL Collaboration), Nucl.Phys.Proc.Suppl. **63**, 269 (1998), hep-lat/9710050.
[7] A. O'Cais, K. J. Juge, M. J. Peardon, S. M. Ryan, and J.-I. Skullerud (TrinLat Collaboration), Nucl.Phys.Proc.Suppl. **140**, 844 (2005), hep-lat/0409069.
[8] J. Foley, K. Jimmy Juge, A. O'Cais, M. Peardon, S. M. Ryan, et al., Comput.Phys.Commun. **172**, 145 (2005), hep-lat/0505023.
[9] C. Alexandrou, K. Hadjiyiannakou, G. Koutsou, A. O'Cais, and A. Strelchenko, Comput.Phys.Commun. **183**, 1215 (2012), 1108.2473.
[10] S. Collins, G. Bali, and A. Schafer, PoS **LAT2007**, 141 (2007), 0709.3217.
[11] G. S. Bali, S. Collins, and A. Schafer, Comput.Phys.Commun. **181**, 1570 (2010), 0910.3970.
[12] C. McNeile and C. Michael (UKQCD Collaboration), Phys.Rev. **D63**, 114503 (2001), hep-lat/0010019.
[13] R. Frezzotti, P. A. Grassi, S. Sint, and P. Weisz (Alpha), JHEP **0108**, 058 (2001), hep-lat/0101001.
[14] R. Frezzotti and G. C. Rossi, Nucl. Phys. Proc. Suppl. **128**, 193 (2004), hep-lat/0311008.
[15] R. Frezzotti and G. C. Rossi, JHEP **08**, 007 (2004), hep-lat/0306014.
[16] R. Frezzotti and G. C. Rossi, JHEP **10**, 070 (2004), hep-lat/0407002.
[17] C. Alexandrou, M. Constantinou, V. Drach, K. Hadjiyiannakou, K. Jansen, et al. (2013), 1309.2256.
[18] C. Alexandrou, M. Constantinou, S. Dinter, V. Drach, K. Jansen, et al. (2013), 1303.5979.

[19] K. Bitar, A. Kennedy, R. Horsley, S. Meyer, and P. Rossi, Nucl.Phys. **B313**, 377 (1989).
[20] K. Jansen, C. Michael, and C. Urbach (ETM Collaboration), Eur.Phys.J. **C58**, 261 (2008), 0804.3871.
[21] K. Ottnad et al. (ETM collaboration), JHEP **1211**, 048 (2012), 1206.6719.
[22] C. Michael, K. Ottnad, and C. Urbach (2013), 1310.1207.
[23] R. Baron et al., JHEP **06**, 111 (2010), 1004.5284.
[24] L. Maiani, G. Martinelli, M. Paciello, and B. Taglienti, Nucl.Phys. **B293**, 420 (1987).
[25] S. Gusken (1999), hep-lat/9906034.
[26] S. Capitani, B. Knippschild, M. Della Morte, and H. Wittig, PoS **LATTICE2010**, 147 (2010), 1011.1358.
[27] A. Skouroupathis and H. Panagopoulos, Phys.Rev. **D79**, 094508 (2009), 0811.4264.
[28] B. Blossier et al. (ETM Collaboration), PoS **LATTICE2011**, 233 (2011), 1112.1540.
[29] ETMC (European Twisted Mass Collaboration), in preparation.
[30] C. Alexandrou, M. Constantinou, T. Korzec, H. Panagopoulos, and F. Stylianou, Phys.Rev. **D83**, 014503 (2011), 1006.1920.
[31] C. Alexandrou, M. Constantinou, T. Korzec, H. Panagopoulos, and F. Stylianou, Phys.Rev. **D86**, 014505 (2012), 1201.5025.
[32] J. Gracey, Nucl.Phys. **B662**, 247 (2003), hep-ph/0304113.
[33] M. Gong, A. Alexandru, Y. Chen, T. Doi, S. Dong, et al., Phys.Rev. **D88**, 014503 (2013), 1304.1194.
[34] M. Deka, T. Streuer, T. Doi, S. Dong, T. Draper, et al., Phys.Rev. **D79**, 094502 (2009), 0811.1779.
[35] A. Stathopoulos and K. Orginos, SIAM J.Sci.Comput. **32**, 439 (2010), 0707.0131.
[36] A. Stathopoulos, A. Abdel-Rehim, and K. Orginos, J.Phys.Conf.Ser. **180**, 012073 (2009).